J Mater Sci

Electronic materials

Fast X-ray detectors based on bulk β-Ga_2O_3 (Fe)

Ibrahim Hany[1], Ge Yang[1,*], and Ching-Chang Chung[2]

[1] *Department of Nuclear Engineering, North Carolina State University, Raleigh, NC 27607, USA*
[2] *Analytical Instrumentation Facility, North Carolina State University, Raleigh, NC 27695, USA*

Received: 28 December 2019
Accepted: 8 April 2020

© Springer Science+Business Media, LLC, part of Springer Nature 2020

ABSTRACT

(010) EFG-grown Fe-doped β-Ga_2O_3 was tested as a low-noise X-ray detector with Ti/Au electrodes vertical structure. Its performance at low, high and no applied voltages was examined. The fabricated detector showed high X-ray detection performance manifested in its signal's short fall and rise time (< 0.3 s) in all operation modes, showing two orders of magnitude decrease in response time of β-Ga_2O_3 X-ray detectors. The same temporal response was exhibited by a tested Au/Ni/β-Ga_2O_3/Ti/Au device. The detector's signal is also characterized by excellent linear relation with X-ray tube current and high signal-to-noise ratio (SNR) optimized at -5 V ($> 10^3$). Moreover, the X-ray-induced current signal exhibits high stability. Sub-band UV photocurrent signal showed a significantly slower response compared to X-ray-induced conductivity signal. Possible charge transport mechanisms involving ion migration are suggested and discussed. In this study, Fe doping is shown to significantly improve X-ray detection performance of Ga_2O_3, consolidating the applicability of Ga_2O_3 as a next-generation X-ray detector functioning with low power, high SNR and linearity, and significantly improved transient characteristics.

Introduction

β-Ga_2O_3 possesses multiple superior material properties including high thermal stability, ultra-wide bandgap, high device breakdown voltage, n-conductivity controllability, excellent radiation hardness and fabrication versatility [1–5]. Such characteristics are currently paving the road for high-performance devices based on β-Ga_2O_3 in power electronics [2], UV photodetection [3], gas detection, indirect radiation detection [6–8] and neutron detection [9]. Moreover, β-Ga_2O_3's relatively high density (6.44 gm/cm^3) in addition to its high radiation resistance attracts strong attention as a candidate X-ray detector with exceptionally high performance in harsh environments. Recently, β-Ga_2O_3 Schottky barrier diode (SBD) as well as amorphous Ga_2O_3 (a-Ga_2O_3) flexible metal–semiconductor–metal (MSM) X-ray detectors have shown high X-ray responsivity and linearity [10–12]. SBD suffered from long response time ($\tau_{r1,\ d1} > 10$ s) under -10 V reverse bias which was significantly shortened in the absence of bias voltage. MSM as well as UV sensors [3] based on β-Ga_2O_3 have long transient characteristics as

Address correspondence to E-mail: gyang9@ncsu.edu

https://doi.org/10.1007/s10853-020-04665-9

Springer

Published online: 22 April 2020

well, and photo-persistent current (PPC) is often encountered. This problem should be solved for successful X-ray or photodetector implementation. In this work, we report on the successful development of a fast, stable, high signal-to-noise ratio (SNR) and linear X-ray detector based on Fe-doped β-Ga_2O_3 bulk single crystal operating in low and high electric fields as well as self-powered mode.

Experimental

(010) EFG Fe-doped β-Ga_2O_3 with 5×5 mm^2 surface area and 0.5 mm thickness was used as the active detector material. 4×4 mm^2 Ti/Au (50/50 nm) contacts were deposited on each side after cleaning with acetone. For better contact formation, the device was annealed for 10 min at 400 °C in air. More details on device fabrication and its electrical and optical characterization can be found in our previous report [13]. The X-ray-induced conductivity experimental setup is shown in Fig. 1a. The X-ray tube (Cu, 45 kV, 40 mA) was equipped in a X-ray diffractometer (Empyrean, PANalytical), and no optics were used in front of the beam other than a mask and a Soller slit which were used to define the beam geometry. A Keithley 6487 source measure unit (SMU) was used to apply the external electric field and measure the induced current. The temporal X-ray-induced conductivity was measured in 0.3 s steps. Another Au (50 nm)/Ni (40 nm)/β-Ga_2O_3/Ti (50 nm)/Au (50 nm) device was fabricated using the same procedures followed for the primarily studied device. We used UV LED (365 nm) for photoconductivity transient measurements. Time of flight–secondary ion mass spectroscopy (TOF–SIMS) analyses were conducted using a TOF SIMS V (ION TOF, Inc. Chestnut Ridge, NY) instrument. The surface was sputtered with 10 keV Cs^+ beam at 30 nA for 20 scans over 550 μm × 550 μm area, which only sputtered away a few nanometers of β-Ga_2O_3 (Fe), mainly surface contaminations. Analysis beam was 25 keV $Bi_3{}^+$ ion at 0.15 pA current.

Results and discussion

A small detector thickness is preferred from the standpoint of charge collection efficiency and detector fabrication. Thus, an ideal candidate X-ray sensing material should have high attenuation coefficient. Figure 1b shows the linear attenuation coefficient (for incoherent scattering [14]) of Ga_2O_3, compared with other semiconductor X-ray sensing materials. Other than lead compounds, the linear attenuation coefficient of Ga_2O_3 is among the highest exhibited by these currently studied semiconductor X-ray detector materials. Particularly, gallium compounds have early L and K edges improving their attenuation relative to those compared materials around these energies.

The current–voltage (I–V) behavior was studied in our previous report and is presented here in Fig. 1c [13]. Au/Ti/β-Ga_2O_3 (Fe)/Ti/Au showed a near-Ohmic behavior and demonstrated a high resistivity close to 9.1×10^{13} Ω cm, which would lead to an enhanced SNR and thus motivated our efforts to develop Fe-doped β-Ga_2O_3-based radiation detectors.

Self-powered operation

Upon X-ray illumination (45 kV, 40 mA), the device exhibited X-ray-induced conductivity at no external applied voltage with the current reaching − 21 pA as shown in Fig. 1d. For such no bias operation, the dark transient current was − 0.15 (± 0.05) pA, which is close to the SMU resolution. (The testing box cover was open compromising the noise level.) Assuming that a built-in voltage is responsible for the no-bias device operation leaking 0.15 pA, the calculated SNR is 139. More importantly, the rise and fall time of the signal is less than 0.3 s. This operation is expected to be in the photovoltaic mode, where no electrons originating from traps contribute to the signal (no detrapping). To gain insight into the underlying reason for the built-in voltage, we consider three different scenarios. First, it could indicate that the near-Ohmic (no turn-on voltage between − 10 and 10 V) behavior exhibited by the device is indicative of Schottky contact formation. However, the current does not exceed − 10 pA under an applied voltage of − 100 V. Thus, a Schottky contact formation is highly unlikely to be responsible for the built-in voltage. The second possibility is that the built-in voltage was triggered by electron–hole formation from X-ray interaction (photoelectric and Compton scattering) near the irradiated surface. Charge carriers get trapped near the surface by deep-level defects that are potentially abundant near the surface, leading to a built-in electric field. The third possibility is that Fe

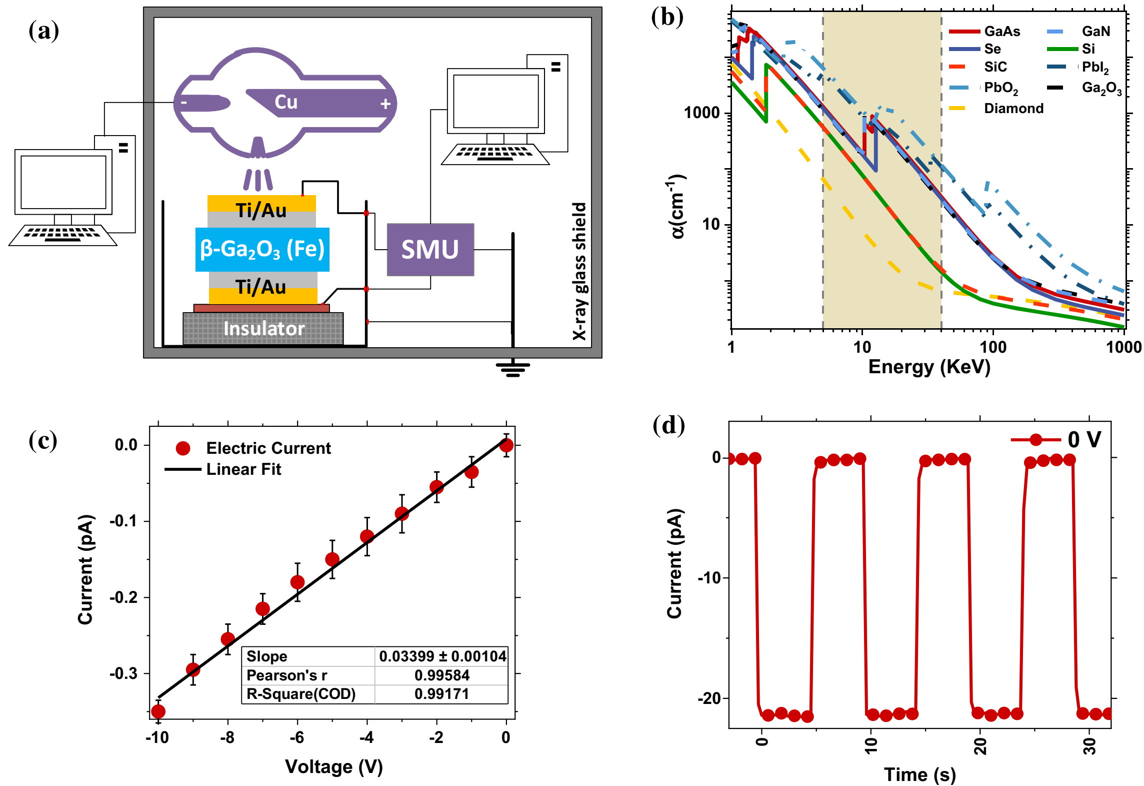

Figure 1 **a** X-ray-induced current measurement schematic setup, **b** linear attenuation coefficient from 1 keV to 1 MeV for Ga_2O_3 compared to a number of current and candidate X-ray sensing materials. The highlighted region denotes energy range used for this study, **c** I–V curve of Fe-doped β-Ga_2O_3 along b-axis, **d** self-powered mode transient response of the device (period = 10 s).

dopants might have a nonuniform distribution throughout the thickness of the β-Ga_2O_3 crystal, leading to built-in voltage. In that case, the built-in voltage arises from the difference in electrons/holes concentrations through the thickness due to nonuniformity of Fe distribution. TOF–SIMS was used to obtain the information of Fe distribution through the thickness of β-Ga_2O_3 (Fe), as shown in Fig. 2, which revealed a nonuniform distribution of Fe doping. This is consistent with the assumption that the nonuniform distribution of Fe in EFG-grown β-Ga_2O_3 (Fe) is the underlying reason for the built-in voltage that allowed the X-ray detector operation under the absence of external applied voltage. From a sensor device viewpoint, the significant SNR and fast timing response show the potential of Fe-doped Ga_2O_3 as a promising X-ray detector for low-power operation.

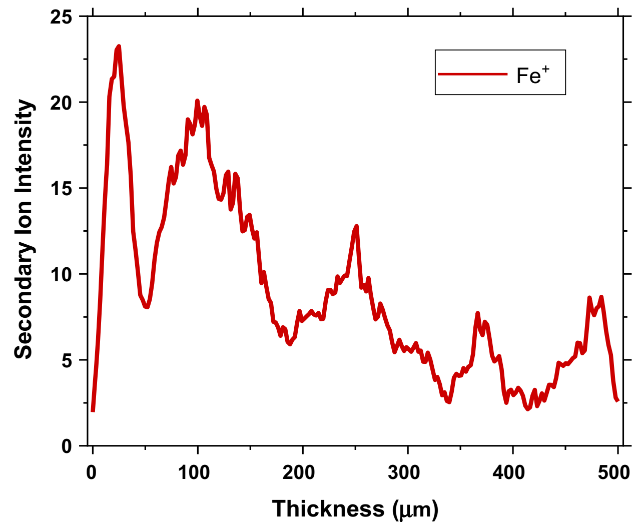

Figure 2 Fe^+ secondary ion intensity through the β-Ga_2O_3 (Fe) thickness obtained by TOF–SIMS.

Temporal response

The device was tested under the low applied voltage of 5 V and − 5 V, respectively. The transient response for 10-s X-ray (45 kV and 40 mA) period is shown in Fig. 3. The device showed no experimental lag in its response ($\tau_r, \tau_f < 0.3$ s) in the presence of low electric field similar to the case when it is absent. Compared to the same positive applied field, the signal was higher under the negative applied field.

To further examine the fast response time stability, the transient operations under − 10 V, − 20 V, − 50 V and − 100 V were examined. The results, shown in Fig. 4a, illustrate that the response time is not deteriorated under high electric fields as well, and it remains below 0.3 s.

To study whether the contact has a role in the device fast signal temporal behavior or not, Au/Ni/β-Ga_2O_3 (Fe)/Ti/Au device was fabricated and the signal exhibited the same fast response as shown in Fig. 5a. We emphasize that the I–V behavior of this device was near-Ohmic as well, which is the same behavior exhibited by the Au/Ti/β-Ga_2O_3 (Fe)/Ti/Au device.

Iron is expected to form Fe_{Ga} deep level around 0.8 eV below conduction band minimum (CBM) [15–17]. The fact that the signal rise and fall time is so fast, compared to undoped Ga_2O_3-based X-ray and photo-detectors, may either indicate that this deep-level band contributes to conduction or that it traps charge carriers without an effective followed detrapping process.

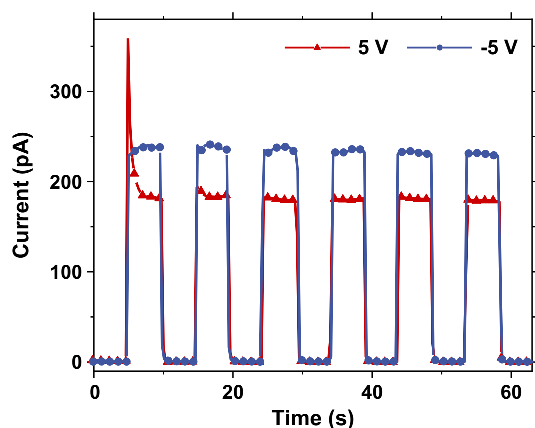

Figure 3 Low-voltage transient response of the device (period = 10 s). The negative current was flipped for illustration.

Signal-to-noise ratio

Considering that the device can be operated under zero, low and high applied voltages, the preferable operating regime should be the one that produces the highest SNR. Furthermore, a high SNR is critical if the operation of the device would be extended to pulse reading mode for energy-resolved X-ray detection. In our treatment, we define SNR as the ratio between the net induced current and the dark current (SNR $= \frac{I_{\text{x-ray induced}} - I_{\text{dark}}}{I_{\text{dark}}}$; $I_{\text{dark}} = \frac{3.2 \times V_{\text{applied}}}{9.1 \times 10^{13}}$; 3.2 is the detector area to length ratio in cm. However, it should be noted that in practical detector operation, sources of signal error include instrumental sources and statistical sources arising from the statistical nature of X-ray interaction with electrons. As shown in the inset of Fig. 4b, the SNR for operating voltages between − 5 and − 50 V stays above 800 and decreases for the higher applied voltages. This indicates that the increase in intrinsic dark current is higher than the increase in the induced current. More importantly, the SNR stays above 1000 for applied voltages between − 5 and − 20 V, and it is further optimized at − 5 V exceeding 1200. These results clearly show that the device possesses better characteristics at low-voltage operation compared to high-voltage region.

To gain more insight about the charge carriers transport properties, the single-carrier Hecht equation fitting was used to estimate the drift length of the effective charge carriers, as shown in Fig. 4b. It should be noted that although single charge carrier is assumed here, this assumption is only made in order to gain a quantitative estimate for the transport properties of charge carriers, and the contribution from both electrons and holes should not be overlooked in highly accurate treatments as both types of charge carriers could contribute to the signal. In fact, the mobility–lifetime product ($\mu\tau$) factor calculated from this rough treatment was 2.28×10^{-5} cm^2/V, which yields 45.6 μm/456 μm carrier drift length for 10 V/100 V, respectively. These values are higher than that obtained from electron beam-induced current (EBIC) for electrons and holes [22–25], suggesting that they both contribute to the signal.

Table 1 shows the characteristic temporal response and SNR of β-Ga_2O_3 (Fe) X-ray detector compared to previously reported Ga_2O_3-based X-ray detectors as well as other X-ray detectors based on wide bandgap

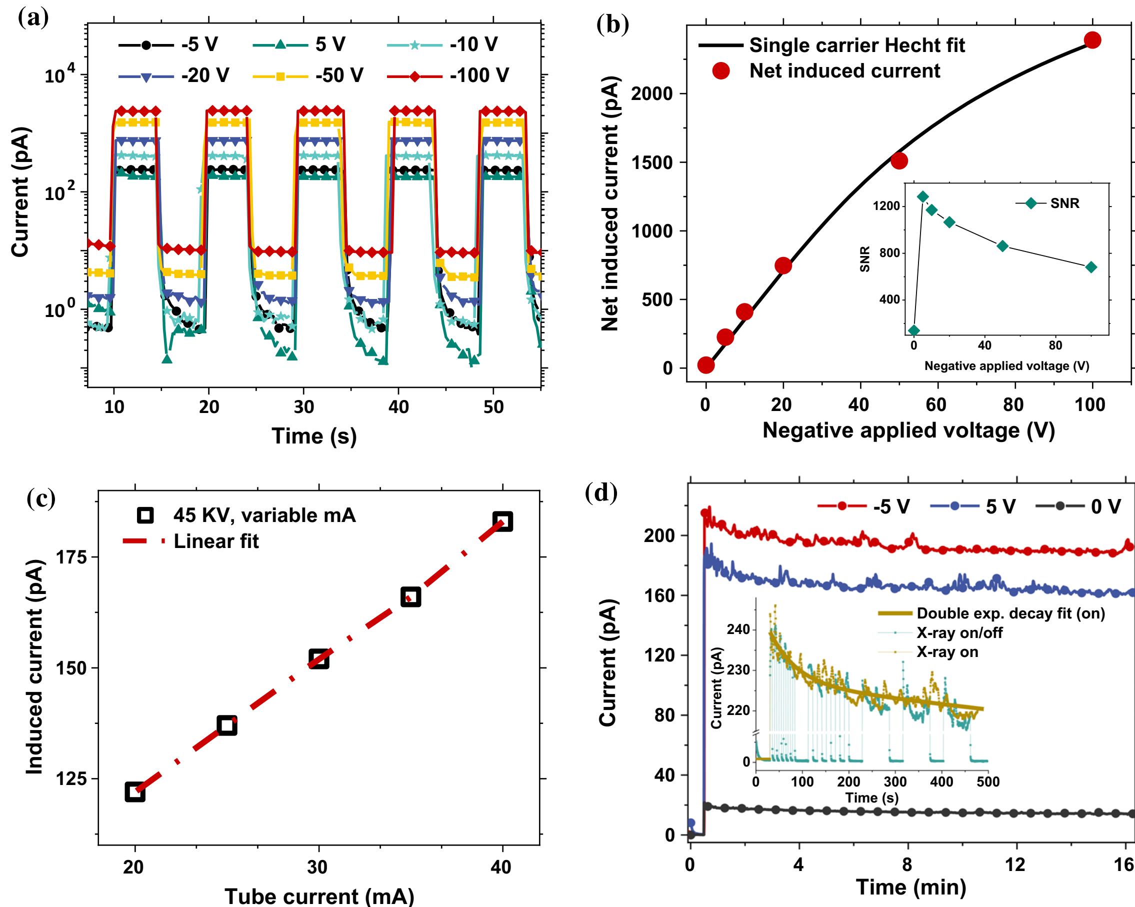

Figure 4 **a** Transient response of the Au/Ti/β-Ga_2O_3 (Fe)/Ti/Au device under low and high applied voltages (period = 10 s). **b** Single charge carrier Hecht fitting [18–21]. The inset shows SNR at tested applied voltages (45 kV, 40 mA). **c** Response current linearity. **d** Stability test for 15 min. The inset shows double exponential decay fitting for 15-min stability test under − 5 V applied voltage with X-ray tube operating at 45KV and 40 mA, compared to ON/OFF testing under the same applied voltage and tube parameters. The negative current was flipped for illustration.

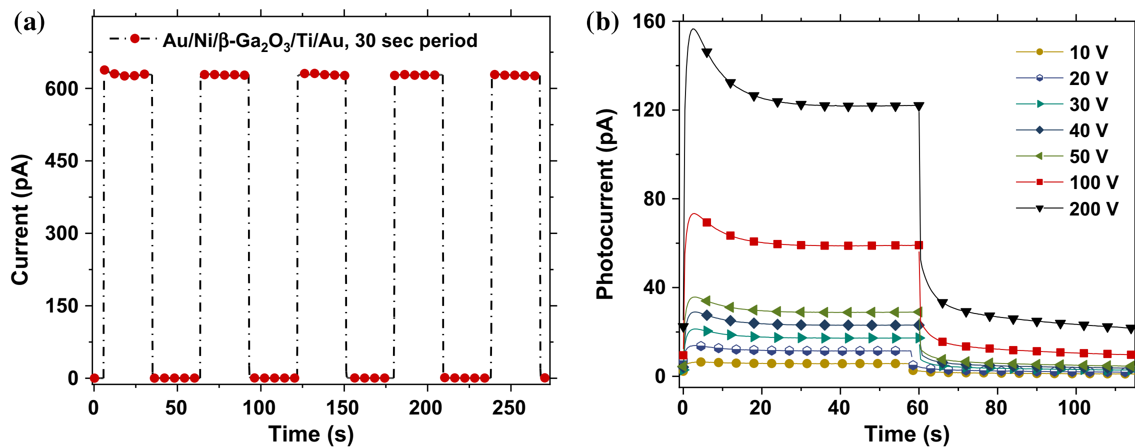

Figure 5 **a** X-ray-induced (45 kV and 40 mA) conductivity transient response for Au/Ni/β-Ga_2O_3/Ti/Au device under 10 V (period = 1 min), **b** sub-band UV transient photoconductivity at different applied voltages (period = 2 min).

Table 1 Comparison of temporal response and SNR ratio of X-ray detectors based on wide bandgap semiconductors, showing the significant improvement in timing characteristics of Fe-doped β-Ga_2O_3-based X-ray detector compared to unintentionally doped β-Ga_2O_3 and amorphous Ga_2O_3, without compromising SNR

Material	Preparation method	Rise time (s)	Decay time (s)	SNR	References
a-Ga_2O_3	RF sputtering (PO_2 1.4×10^{-3} Pa)	15.5	1.1	–	[12]
	RF sputtering (PO_2 1.0×10^{-3} Pa)	50.1	3.3	$> 10^4$	
Unintentionally doped β-Ga_2O_3	EFG	18.3 (– 15 V) < 0.02 (0 V)	20.9 (– 15 V) < 0.02 (0 V)	> 800 (– 15 V) –	[10]
β-Ga_2O_3 (Fe)	EFG	< 0.3	< 0.3	$> 10^3$ (low voltages) $> 10^2$ (0 V and high voltage)	This work
GaN	MOCVD	15	–	< 30	[26]
		< 0.02 (0 V)	< 0.02 (0 V)	< 20	[27]
GaN (Fe)	HVPE	28	2	180	[28]
Zn_2SiO_4	RF sputtering and annealing	< 1	< 1	$> 10^3$	[29]
		~ 30	~ 8	480	[30]
ZnO	RF sputtering	–	~ 0.1	< 5	[31]
	RF sputtering	0.2	0.2	300	[32]

semiconductors. It can be seen that β-Ga_2O_3 (Fe) X-ray response showed approximately two orders of magnitude transient response improvement compared to previously reported Ga_2O_3 X-ray detectors, without compromising SNR. Compared to other wide bandgap X-ray detectors, β-Ga_2O_3 (Fe) shows outstanding compromise between the transient response and SNR, especially under low applied voltages, which can be achieved using 5 V batteries.

Linearity

The X-ray tube power was varied by changing the tube current at constant tube voltage under – 5 V applied voltage in order to test the device response linearity. As shown in Fig. 4c, the X-ray-induced current response is highly linear with the current of the X-ray tube. Such linear response encourages further investigation on operating the device in the pulse mode (potentially low-power X-ray spectrometer) as well as in the current mode (X-ray counter as in regular imagers with very high dynamic range when operated at high voltage).

Stability

Continuous X-ray (40 kV, 40 mA)-induced conductivity measurements were conducted for 15 min at 5 V, – 5 V and 0 V to assess the device response stability. As shown in Fig. 4d, the device shows very high stability at tested operating voltages, all with the same fast rise time. However, a closer look to the signal time behavior reveals small exponential decay within the first minute that stabilizes after that. The inset of Fig. 4d shows a double exponential decay fitting for the continuous X-ray time-dependent response (– 5 V, 45 KV, 40 mA), resulting in $\tau_1 =$ 57.7 s and $\tau_2 > 10^6$ s (stability). Two possible scenarios can be responsible for this behavior.

First, the poor heat conduction of β-Ga_2O_3 may have caused a slight increase in the sample temperature due to device operation such as X-ray material interaction and charge flow in the device when the bias voltage is applied. This temperature increase deteriorates the transport properties of charge carriers, as illustrated by previous EBIC studies, which would lead to a decrease in the induced current [22–25]. In this scenario, the total drop in the current should significantly differ at different operating voltages, with higher drop at higher voltages, and/or higher X-ray power. Moreover, the detector under continuous operation should suffer from continuous induced current drop, which is not the case in our study. Thus, we exclude that the poor thermal conductivity was the reason behind this effect.

The second scenario can be triggered by space charge accumulation on the surface near the electrodes, causing an internal electric field opposite to the external applied electric field and leading to slight

polarization effect. In further analysis of this behavior, ionic conductivity of defects (e.g., oxygen vacancies) should be considered.

Comparing the time-dependent evolution of the current under continuous and ON/OFF X-ray illumination under the same measurement conditions, we observed memory effect of the signal, as shown in Fig. 4d inset. In other words, this decay effect is independent of the X-ray illumination state after the initial X-ray pulse, which consolidates the second scenario involving the polarization effect. After the space charge is formed on the semiconductor surface near the electrodes, they stay there as long as the electric field is applied; thus, the electric field is deteriorated and remains this way even in the absence of charge carrier generation. This behavior could be related to ionic migration of oxygen vacancies (ionic conductivity).

Temporal UV photoconductivity under different applied voltages

To investigate the UV photocurrent transient response, the sub-band gap excitement with 365 nm LED (3.4 eV) was used since the band gap of β-Ga_2O_3 (Fe) is 4.45 eV [13]. The UV photoconductivity results are shown in Fig. 5b. 10–90% rise/fall time improved from 2 s/16 s at 5 V to 1 s/10 s at 200 V, and the photocurrent had a linear dependency with applied voltage (unlike the X-ray-induced current voltage dependence that follows Hecht model). The enhanced transient and charge carrier transport properties of the X-ray-induced current (compared to sub-band UV photocurrent) are probably caused by the enhanced charge carrier transport properties for charge carriers excited above the deep acceptor level of Fe_{Ga}, often referred as E_2 ($\sim$ 0.8 eV below CBM) [16, 17] in the case of X-ray-induced response.

Conclusion

Fe-doped β-Ga_2O_3 was investigated as a direct X-ray detection material motivated by its high resistivity and ultra-low leakage current. β-Ga_2O_3 (Fe) with Ti/Au electrodes demonstrated high SNR under three operation modes including low applied voltage ($>$ 1200 at $-$ 5 V), high applied voltage ($>$ 650 at $-$ 100 V) and self-powered operation mode ($>$ 100). We also observed high linearity between X-ray-induced photocurrent and X-ray tube current. More importantly, the signal's rise and fall time was below 0.3 s, which offers excellent measurement time resolution. This fast response was independent of the applied voltage and was not electrode dependent, as indicated by the fact that the response did not deteriorate upon testing a Au/Ni/β-Ga_2O_3 (Fe)/Ti/Au device. The device showed high stability upon continuous illumination for 15 min with an exponential decay behavior ($\tau = 57.7$ s) which stabilizes shortly after that. The sub-band photocurrent measurements showed significantly slower transient response. Further investigations of the device response to UV light, especially in the energy range between E_2 and CBM band (3.65 to 4.45 eV), are necessary to evaluate the device performance as solar-blind deep UV sensor. Analysis of β-Ga_2O_3 (Fe) X-ray detector characteristics including charge carrier transport suggests that both holes and electrons contribute to the signal formation and that a slight polarization effect takes place. The results demonstrate the great potential of β-Ga_2O_3 (Fe) as a radiation-resistant X-ray detector with excellent temporal response for a wide range of applications.

Acknowledgements

We would thank the support from the U.S. Nuclear Regulatory Commission (NRC). This work was performed in part at the Analytical Instrumentation Facility (AIF) at North Carolina State University, which is supported by the State of North Carolina and the National Science Foundation (Award Number ECCS-1542015). The AIF is a member of the North Carolina Research Triangle Nanotechnology Network (RTNN), a site in the National Nanotechnology Coordinated Infrastructure (NNCI).

Compliance with ethical standards

Conflict of interest The authors declare that they have no conflict of interest.

References

[1] Zhou H, Zhang J, Zhang C, Feng Q, Zhao S, Ma P, Hao Y (2019) A review of the most recent progresses of state-of-art gallium oxide power devices. J Semicond 40:11803. https://doi.org/10.1088/1674-4926/40/1/011803

[2] Liu Z, Li PG, Zhi YS, Wang XL, Chu XL, Tang WH (2019) Review of gallium oxide based field-effect transistors and Schottky barrier diodes. Chin Phys B 28:17105. https://doi.org/10.1088/1674-1056/28/1/017105

[3] Chen X, Ren F, Gu S, Ye J (2019) Review of gallium-oxide-based solar-blind ultraviolet photodetectors. Photonics Res 7:381–415. https://doi.org/10.1364/prj.7.000381

[4] Pearton SJ, Yang J, Cary PH, Ren F, Kim J, Tadjer MJ, Mastro MA (2018) A review of Ga_2O_3 materials, processing, and devices. Appl Phys Rev 5:011301. https://doi.org/10.1063/1.5006941

[5] Tadjer MJ, Lyons JL, Nepal N, Freitas JA, Koehler AD, Foster GM (2019) Review—theory and characterization of doping and defects in β-Ga_2O_3. ECS J Solid State Sci Technol 8:Q3187–Q3194. https://doi.org/10.1149/2.0341907jss

[6] Usui Y, Nakauchi D, Kawano N, Okada G, Kawaguchi N, Yanagida T (2018) Scintillation and optical properties of Sn-doped Ga_2O_3 single crystals. J Phys Chem Solids 117:36–41. https://doi.org/10.1016/j.jpcs.2018.02.027

[7] He N, Tang H, Liu B, Zhu Z, Li Q, Guo C, Gu M, Xu J, Liu J, Xu M, Chen L, Ouyang X (2018) Ultra-fast scintillation properties of β-Ga2O3 single crystals grown by Floating Zone method. Nucl Instrum Methods Phys Res Sect A Accel Spectrometers Detect Assoc Equip 888:9–12. https://doi.org/10.1016/j.nima.2018.01.023

[8] Makowski M, Drozdowski W, Witkowski ME, Wojtowicz AJ, Irmscher K, Schewski R, Galazka Z (2019) Tailoring the scintillation properties of β-Ga_2O_3 by doping with Ce and codoping with Si. Opt Mater Express 9:3738–3743. https://doi.org/10.1364/ome.9.003738

[9] Szalkai D, Galazka Z, Irmscher K, Tutto P, Klix A, Gehre D (2017) β-Ga_2O_3 solid-state devices for fast neutron detection. IEEE Trans Nucl Sci 64:1574–1579. https://doi.org/10.1109/TNS.2017.2698831

[10] Lu X, Zhou L, Chen L, Ouyang X, Liu B, Xu J, Tang H (2018) Schottky x-ray detectors based on a bulk β-Ga_2O_3 substrate. Appl Phys Lett 112:103502. https://doi.org/10.1063/1.5020178

[11] Lu X, Zhou L, Chen L, Ouyang X, Tang H, Liu B, Xu J (2019) X-ray detection performance of vertical schottky photodiodes based on a bulk β-Ga_2O_3 substrate grown by an EFG method. ECS J Solid State Sci Technol 8:Q3046–Q3049. https://doi.org/10.1149/2.0071907jss

[12] Liang H, Cui S, Su R, Guan P, He Y, Yang L, Chen L, Zhang Y, Mei Z, Du X (2019) Flexible x-ray detectors based on amorphous Ga_2O_3 thin films. ACS Photon 6:351–359. https://doi.org/10.1021/acsphotonics.8b00769

[13] Hany I, Yang G, Zhou CE, Sun C, Gundogdu K, Seyitliyev D, Danilov EO, Castellano FN, Sun D, Vetter E (2019) Low temperature cathodoluminescence study of Fe-doped β-Ga_2O_3. Mater Lett 257:126744. https://doi.org/10.1016/j.matlet.2019.126744

[14] Berger MJ, Hubbell JH, Seltzer SM, Chang J, Coursey JS, Sukumar R, Zucker DS, Olsen K (2010) XCOM: photon cross section database (version 1.5), XCOM Phot. Cross Sect. Database (Version 1.5). https://physics.nist.gov/xcom. Accessed 3 Dec 2019

[15] Polyakov AY, Smirnov NB, Shchemerov IV, Pearton SJ, Ren F, Chernykh AV, Kochkova AI (2018) Electrical properties of bulk semi-insulating β-Ga_2O_3 (Fe). Appl Phys Lett 113:142102. https://doi.org/10.1063/1.5051986

[16] Ingebrigtsen ME, Varley JB, Kuznetsov AY, Svensson BG, Alfieri G, Mihaila A, Badstübner U, Vines L (2018) Iron and intrinsic deep level states in Ga_2O_3. Appl Phys Lett 112:042104. https://doi.org/10.1063/1.5020134

[17] Polyakov AY, Smirnov NB, Schemerov IV, Chernykh AV, Yakimov EB, Kochkova AI, Tereshchenko AN, Pearton SJ (2019) Electrical properties, deep levels and luminescence related to Fe in bulk semi-insulating β-Ga_2O_3 doped with Fe. ECS J Solid State Sci Technol 8:Q3091–Q3096. https://doi.org/10.1149/2.0171907jss

[18] Lin W, Stoumpos CC, Liu Z, Das S, Kontsevoi OY, He Y, Malliakas CD, Chen H, Wessels BW, Kanatzidis MG (2017) TlSn2I5, a robust halide antiperovskite semiconductor for γ-ray detection at room temperature. ACS Photonics 4:1805–1813. https://doi.org/10.1021/acsphotonics.7b00388

[19] Simon M, Ford RA, Franklin AR, Grabowski SP, Menser B, Much G, Nascetti A, Overdick M, Powell MJ, Wiechert DU (2005) Analysis of lead oxide (PbO) layers for direct conversion X-ray detection. IEEE Trans Nucl Sci 52:2035–2040. https://doi.org/10.1109/TNS.2005.856790

[20] Wei H, Fang Y, Mulligan P, Chuirazzi W, Fang HH, Wang C, Ecker BR, Gao Y, Loi MA, Cao L, Huang J (2016) Sensitive X-ray detectors made of methylammonium lead tribromide perovskite single crystals. Nat Photonics 10:333–339. https://doi.org/10.1038/nphoton.2016.41

[21] Hecht K (1932) Zum Mechanismus des lichtelektrischen Primärstromes in isolierenden Kristallen. Zeitschrift Für Phys 77:235–245. https://doi.org/10.1007/BF01338917

[22] Lee J, Flitsiyan E, Chernyak L, Yang J, Ren F, Pearton SJ, Meyler B, Salzman YJ (2018) Effect of 1.5 MeV electron irradiation on β-Ga_2O_3 carrier lifetime and diffusion length. Appl Phys Lett 112:082104. https://doi.org/10.1063/1.5011971

[23] Modak S, Chernyak L, Khodorov S, Lubomirsky I, Yang J, Ren F, Pearton SJ (2019) Impact of electron injection and temperature on minority carrier transport in alpha-irradiated β-Ga_2O_3 Schottky rectifiers. ECS J Solid State Sci Technol 8:Q3050–Q3053. https://doi.org/10.1149/2.0101907jss

[24] Yakimov EB, Polyakov AY, Smirnov NB, Shchemerov IV, Yang J, Ren F, Yang G, Kim J, Pearton SJ (2018) Diffusion length of non-equilibrium minority charge carriers in β-Ga2O3 measured by electron beam induced current. J Appl Phys 123:185704. https://doi.org/10.1063/1.5027559

[25] Yang J, Ren F, Pearton SJ, Yang G, Kim J, Kuramata A (2017) 1.5 MeV electron irradiation damage in β-Ga_2O_3 vertical rectifiers. J Vac Sci Technol B Nanotechnol Microelectron Mater Process Meas Phenom 35:031208. https://doi.org/10.1116/1.4983377

[26] Yao C, Fu K, Wang G, Yu G, Lu M (2012) GaN-based p-i-n X-ray detection. Phys Status Solidi 209:204–206. https://doi.org/10.1002/pssa.201127446

[27] Zhou L, Lu X, Wu J, Jiang H, Chen L, Ouyang X, Lau KM (2019) Self-powered fast-response X-Ray detectors based on vertical GaN p-n Diodes. IEEE Electron Device Lett 40:1044–1047. https://doi.org/10.1109/LED.2019.2914585

[28] Fu K, Yu G, Yao C, Wang G, Lu M, Zhang G (2011) X-ray detectors based on Fe doped GaN photoconductors. Phys Status Solidi Rapid Res Lett 5:187–189. https://doi.org/10.1002/pssr.201105163

[29] He Y, Zhao X, Wang X, Chen L, Peng W, Ouyang X (2015) Characterizations of an X-ray detector based on a Zn_2 SiO_4 film. Sens Actuators A 236:98–103. https://doi.org/10.1016/j.sna.2015.08.022

[30] Zhou L, Guo S, Zhao X, He Y, Chen L, Ouyang X (2019) X-ray detector based on p+-Si/n-Zn_2SiO_4 heterojunction diode. IEEE Photonics Technol Lett 31:1596–1599. https://doi.org/10.1109/LPT.2019.2939054

[31] Liang H-L, Cui S-J, Huo W-X, Wang T, Zhang Y-H, Quan B-G, Du X-L, Mei Z-X (2019) Direct ZnO x-ray detector with tunable sensitivity *. Chin Phys Lett 36:110701. https://doi.org/10.1088/0256-307X/36/11/110701

[32] Zhou L, Huang Z, Zhao X, He Y, Chen L, Xu M, Zhao K, Zhang S, Ouyang X (2019) A high-resistivity ZnO film-based photoconductive X-ray detector. IEEE Photonics Technol Lett 31:365–368. https://doi.org/10.1109/LPT.2019.2894296

Publisher's Note Springer Nature remains neutral with regard to jurisdictional claims in published maps and institutional affiliations.